Available online at www.sciencedirect.com
SCIENCE DIRECT
Earth and Planetary Science Letters 241 (2006) 174–187
EPSL
www.elsevier.com/locate/epsl

Seasonality intensification and long-term winter cooling as a part of the Late Pliocene climate development

Stefan Klotz [a,b,*], Séverine Fauquette [c], Nathalie Combourieu-Nebout [d], Dieter Uhl [a,e], Jean-Pierre Suc [b], Volker Mosbrugger [a]

[a] *Institut für Geowissenschaften, Universität Tübingen, Sigwartstr. 10, 72070 Tübingen, Germany*
[b] *Laboratoire PaléoEnvironnements et PaléobioSphère (UMR 5125 CNRS), Université Claude, Bernard- Lyon 1, 27-43 boulevard du 11 Novembre, 69622 Villeurbanne Cedex, France*
[c] *Institut des Sciences de l'Evolution (UMR 5554 CNRS), Université Montpellier II, Place Eugène Bataillon, 34095 Montpellier Cedex 05, France*
[d] *Laboratoire des Sciences du Climat et de l'Environnement (UMR 1572), L'Orme des Merisiers, Centre de Saclay, 91191 Gif-sur-Yvette Cedex, France*
[e] *Laboratory of Palaeobotany and Palynology, Department of Palaeoecology, University of Utrecht, Budapestlaan 4, 3584 CD Utrecht, The Netherlands*

Received 16 March 2005; received in revised form 15 September 2005; accepted 5 October 2005
Available online 21 November 2005
Editor: H. Elderfield

Abstract

A mutual climatic range method is applied to the Mediterranean marine pollen record of Semaforo (Vrica section, Calabria, Italy) covering the period from ~2.46 Ma to ~2.11 Ma. The method yields detailed information on summer, annual and winter temperatures and on precipitation during the nine obliquity and precession-controlled 'glacial' periods (marine isotope stages 96 to 80) and eight 'interglacial' periods (marine isotope stages 95 to 81) characterising this time interval. The reconstruction reveals higher temperatures of at least 2.8 °C in mean annual and 2.2 °C in winter temperatures, and 500 mm in precipitation during the 'interglacials' as compared to the present-day climate in the study area. During the 'glacials', temperatures are generally lower as compared to the present-day climate in the region, but precipitation is equivalent. Along the consecutive 'interglacials', a trend toward a reduction in annual and winter temperatures by more than 2.3 °C, and toward a higher seasonality is observed. Along the consecutive 'glacials', a trend toward a strong reduction in all temperature parameters of at least 1.6 °C is reconstructed. Climatic amplitudes of 'interglacial–glacial' transitions increase from the older to the younger cycles for summer and annual temperatures. The cross-spectral analyses suggest obliquity related warm/humid–cold/dry 'interglacial–glacial' cycles which are superimposed by precession related warm/dry– cold/humid cycles. A time displacement in the development of temperatures and precipitation is indicated for the obliquity band by temperatures generally leading precipitation change at ~4 kyr, and on the precession band of ~9.6 kyr in maximum.

Keywords: Late Pliocene; obliquity; precession; palaeoclimate; pollen

1. Introduction

Research into the Late Pliocene climate is of especial interest as it contributes to the understanding of

* Corresponding author. Institut für Geowissenschaften, Universität Tübingen, Sigwartstr. 10, 72070 Tübingen Germany. Tel.: +49 7071 2973081; fax: +49 7071 295217.
E-mail address: stefan.klotz@uni-tuebingen.de (S. Klotz).

0012-821X
doi:10.1016/j.epsl.2005.10.005

the nature and the processes of global cooling that evolved since the Miocene and intensified after ~2.8 million years ago, exhibiting an alternation of warm ('interglacial') and cool-temperate ('glacial') periods (e.g., [1-6]). The Late Pliocene palaeoclimate response of the Mediterranean is well documented by marine proxy data [7–11] and few vegetation records [6,12, 13]. The marine data revealed the strong influence of the ~41 kyr obliquity periodicity dominantly affecting high latitude climate and leaving its signature in less pronounced 'interglacial–glacial' cycles [14], and the ~23 kyr precession periodicity mainly influencing lower latitude monsoonal activity [11]. Especially, it has been shown that Sea Surface Temperature changes in the Mediterranean were obliquity-controlled and caused by 'interglacial–glacial' variability, whereas Sea Surface Productivity and Salinity changes were precession-controlled and associated with sapropel formation [9,15]. The latter were interpreted as reflecting the influence of the African monsoon. In addition, in a high-resolution marine pollen record of the Semaforo section (Calabria, Italy) covering MIS 96 to 89 (~2.3 to ~2.17 Ma) [5,16], the alternation between warm humid 'interglacials' (obliquity maxima) and cold-temperate dry 'glacials' (obliquity minima) was documented, the cycles of which were assumed to be superimposed by relatively warm humid conditions at times of precession minima and cold dry conditions during precession maxima [15]. So far, however, quantification of terrestrial temperature and precipitation changes on orbital scales are rather sparse for the Late Pliocene, especially in the Mediterranean. The main reason may be first the very few available (relative high-resolution) terrestrial palaeoclimate archives, such as pollen records. In addition, reconstruction methods are required which do not consider modern analogue floras since for older periods (i.e. pre Mid-Pleistocene) frequently floras exist which have no present-day equivalents. Therefore, potentially mutual climatic range methods are applicable (e.g., [17-21]) which determine the ranges of the climatic tolerances of fossil floras by means of the mutual present-day ranges of the nearest living relatives (NLR) of the plants represented in the fossil assemblages. However, so far the climatic resolution is often low with these methods and the databases of the climate requirements of the present-day nearest living relatives of fossil plants are often poor. Hence, we performed a sophisticated mutual climatic range method to provide quantitative temperature and precipitation estimates for the extended data set of the Semaforo pollen record [22] covering the interval of MIS 96 to 80, and to analyse the reconstruction results for palaeoclimatic characteristics. Specifically, we address the following questions: (1) which main climatic trends related to atmospherical changes characterise the successive Late Pliocene cold and warm phases, and (2) how do the vegetation pattern and the reconstructed climate parameters correspond to the obliquity and precession signals?

2. The marine record of Semaforo and its chronology

The Semaforo section contains a marine record exposed South of Crotone/Italy (39°N, 16°42′E) (Fig. 1). The record consists of 180 m of marine clays, comprising 8 sapropel layers (layers 222 to 204 after Hilgen [14]) and 3 volcanic ash beds (near sapropel layers 222, 208, 206). The time stratigraphic frame of the Semaforo record is well established by astronomically tuned sapropel chronology used for the standard geologic time scale, as well as the standard isotope stratigraphy [15,16,23], suggesting to cover the time span from ~2.46 to ~2.11 Ma (Fig. 2). With respect to the international agreement placing the Pliocene–Pleistocene boundary near the top of the Olduvai subchron at 1.086 Ma as defined in the overlying Vrica section/Italy [23,24], the Semaforo section belongs to the Late Pliocene, the Gelasian Stage. Palynologically, the record is represented in

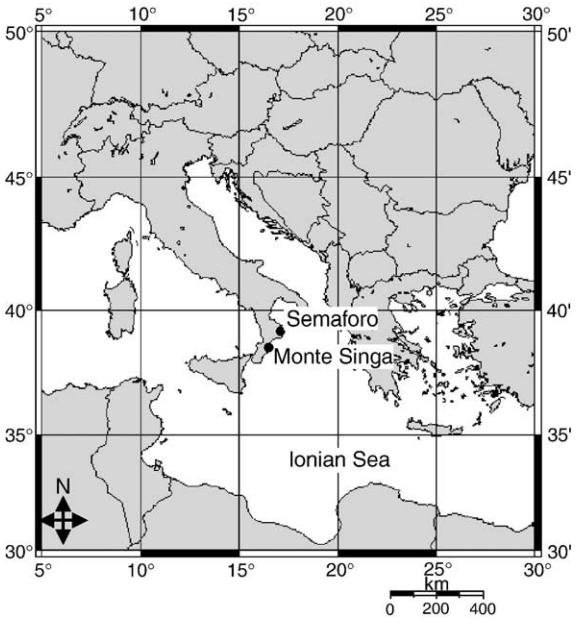

Fig. 1. Site map of the study area with the sections Semaforo and Monte Singa.

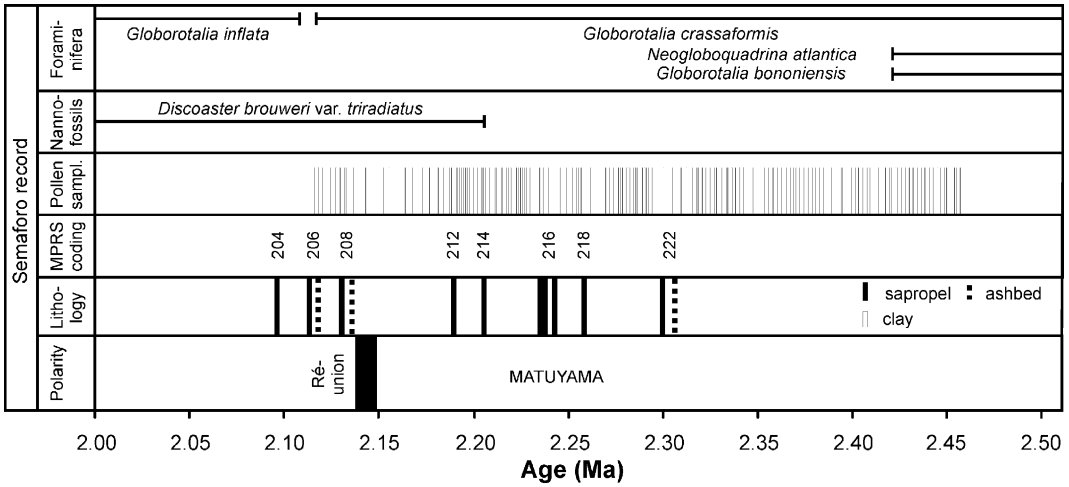

Fig. 2. Stratigraphic column with chronology, polarity zones and lithology [16], MPRS coding [14], pollen samples and biostratigraphy [16].

165 pollen spectra with 110 taxa identified, sampled along 175 m of sediments on intervals between 0.7 and 2 m [16]. For each sample which has been processed according to the standard HF method [25], a number between 200 and 1400 pollen grains have been counted, and abundances have been plotted into a pollen diagram (Fig. 3). The pollen floras sensitively reflect the palaeoclimate development of 'interglacial–glacial' cycles during the Late Pliocene by the repetitive alteration of main vegetation units. These units, which are grouped with respect to the phytogeographical affinities of plants, repeatedly change from deciduous forest (main abundant taxa are *Quercus*, *Acer*, *Ilex*, *Carpinus*, *Buxus*, *Eucommia*, *Carya*, *Juglans*, *Pterocarya*, *Ulmus*) to subtropical humid forest (*Cathaya*, *Engelhardia*, *Magnolia*, *Nyssa*, *Symplocos*, *Taxodiaceae*), to altitudinal forest (*Tsuga*, *Cedrus*, *Picea*, *Abies*), and to open herbaceous formation (Chenopodiaceae, Poaceae, *Artemisia*, *Ephedra*, Asteraceae). Another vegetation unit is represented by Mediterranean ecosystems (*Olea*, *Ceratonia*, *Pistacia*, *Quercus ilex*, *Cistus*, *Phillyrea*, *Ligustrum*), which irregularly follows deciduous forest or subtropical humid forest (Fig. 4). From the base to the top of the fossil pollen record, subtropical humid forest elements (especially Taxodiaceae) are increasingly replaced by deciduous forest elements (especially *Quercus*), until the subtropical ecosystems finally disappear in the Mediterranean at ~1.2 Ma [5,22]. Simultaneously, a general increase in altitudinal forest elements and *Artemisia* as an indicator for open vegetation is observed, but tree pollen always dominate over herbaceous pollen. Climatically, this pattern has been interpreted to suggest (1) that 'interglacial' temperature maxima may decrease during the course of the Late Pliocene, (2) that aridity or seasonality increases, (3) that 'glacial' times experienced enhanced aridity, and (4) that precipitation decreases later than temperatures during 'interglacial–glacial' transitions [16,22].

3. Method used for palaeoclimate reconstruction

For a sophisticated interpretation of palaeoclimate signals, the "probability mutual climatic spheres" (PCS) described in detail by Klotz [20] and Klotz et al. [21,28] is applied, taking into account 60 out of 110 taxa identified in the fossil pollen floras for reconstruction (Table 1). The principle of PCS is based on the calculation of palaeoclimate ranges for a fossil flora by means of mutual 2-dimensional climatic spheres of the NLR of the individual plants which participate in the fossil flora. The 2-dimensional spheres representing the present-day climate requirements of the NLR are derived from the correlation of present-day climate data with digitised potential distribution maps of plants. Within the mutual 2-dimensional climatic sphere of a fossil flora, probability intervals are calculated for the individual climate parameters. For explanation, we refer to mean annual temperature (MAT) as an example. First, the range of MAT as inferred from the mutual climatic sphere of the fossil flora is compared to those MAT ranges which have been calculated for 9555 present-day floras, and for which present-day climate data are available. It can be observed that the actual MAT values of those present-day floras which have similar ranges as the fossil flora accumulate within a smaller interval of the total range, indicating the climatic

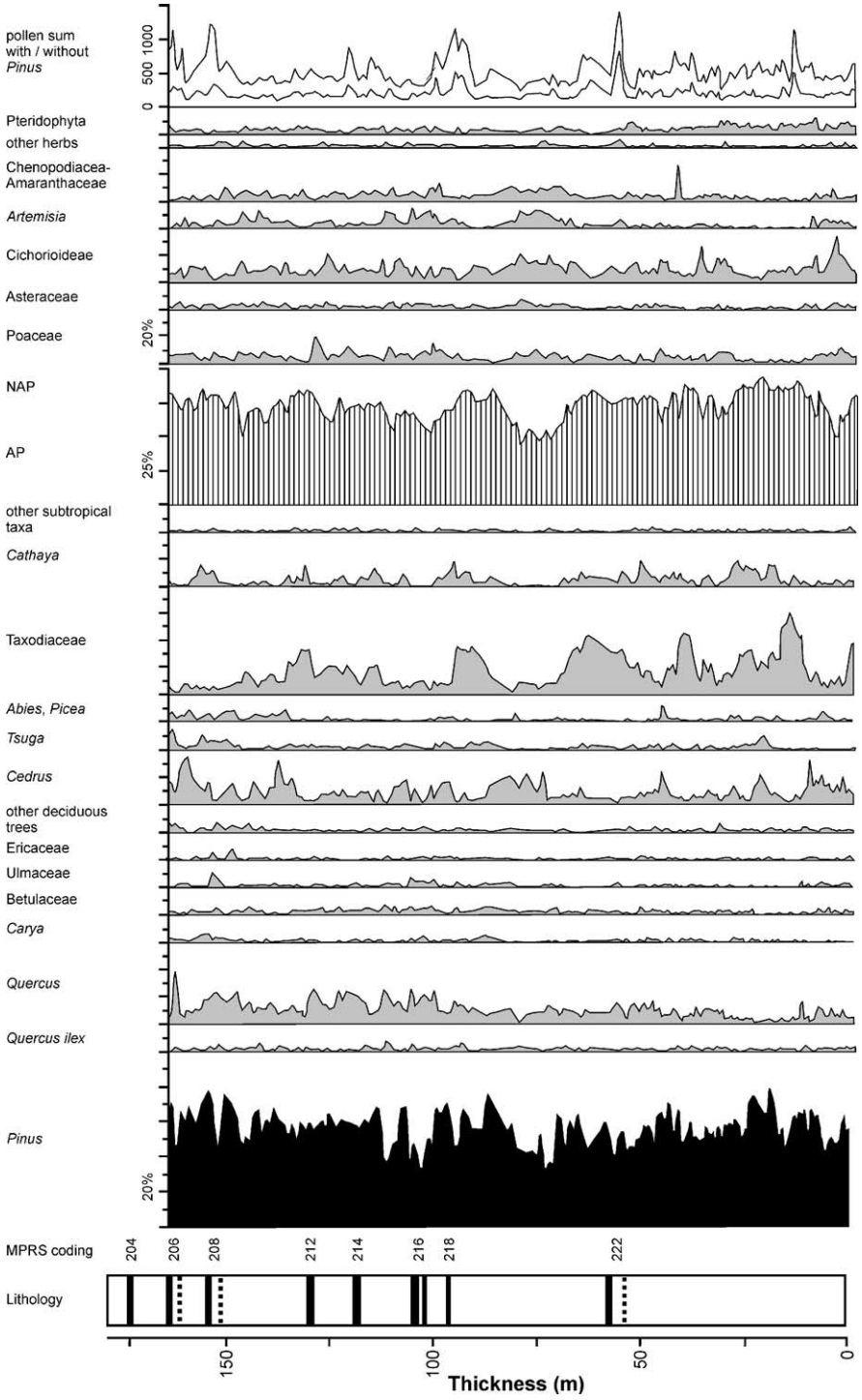

Fig. 3. Pollen diagram of the Semaforo record according to Combourieu-Nebout [22] with thickness, lithology [16] (same caption as in Fig. 2) and MPRS coding [14]. Percentages of *Pinus* are calculated on the total pollen and spores sum, percentages of other taxa and AP, NAP are based on the total sum excluding *Pinus*.

preference of the floras. The interval of preference is then interpreted as the probability interval of MAT. For representation of the reconstructions, we use the centres of the probability intervals. The quality of PCS has been tested on the base of a multitude of present-day floras [20,21], yielding information on the large

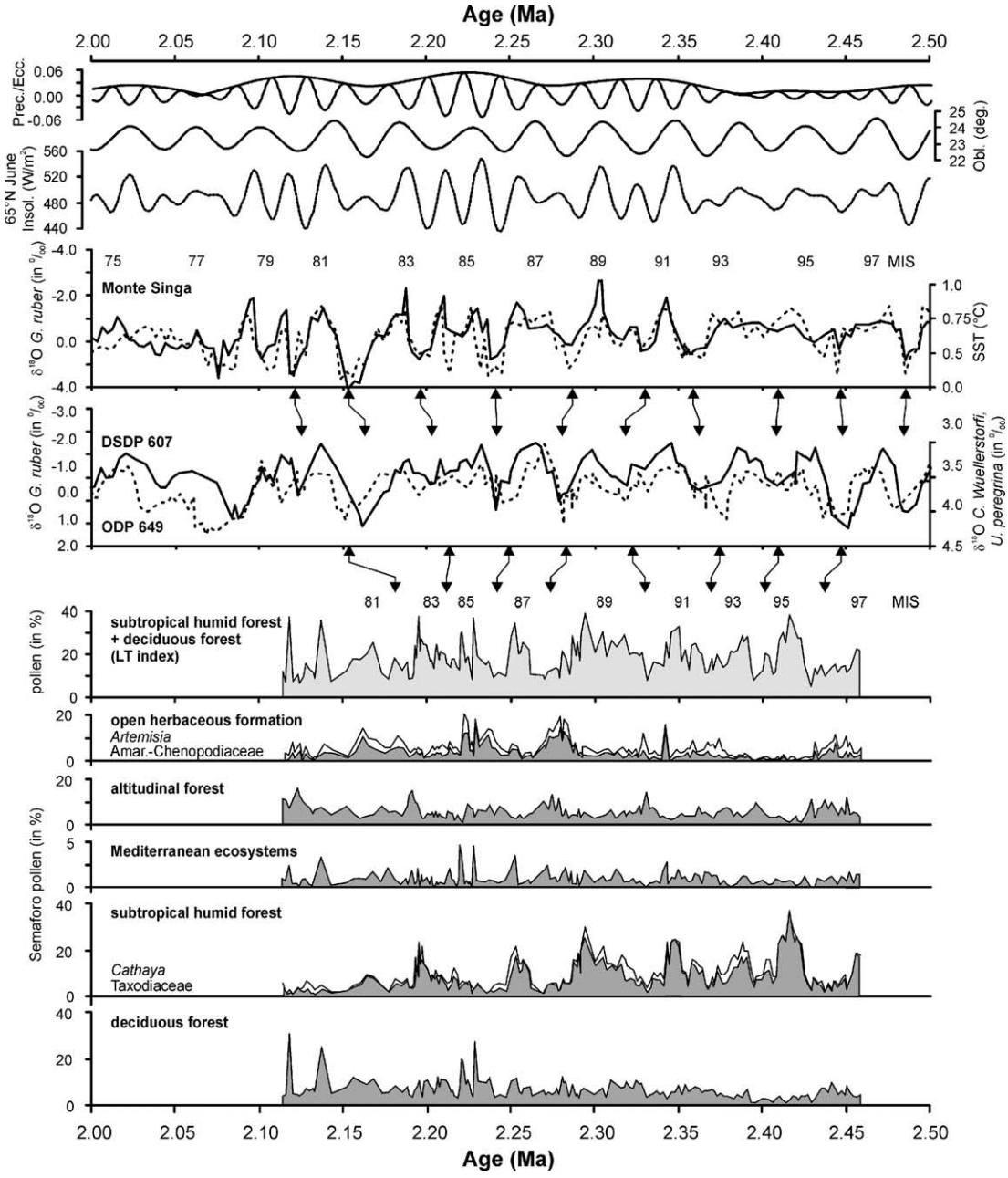

Fig. 4. Generalised pollen diagram of the Semaforo record represented by the percentages of the main vegetation units deciduous forest, subtropical humid forest (most abundant taxa are Taxodiaceae and *Cathaya*), Mediterranean ecosystems, altitudinal forest, and open herbaceous formation (most abundant taxa are Amaranthaceae–Chenopodiaceae and *Artemisia*). Abundance of subtropical humid+deciduous forest reflects a qualitative land temperature (LT) index according to Lourens [15]. Correlation of the Semaforo pollen record with relevant marine indices: The LT index, Sea Surface Temperatures (SST) and planktonic δ^{18}O data from the Singa section (38°3′N, 16°3′W, ~100 km South South–West of Semaforo) [9], and benthic δ^{18}O record from DSDP 607 in the North Atlantic [1] are tied in the lower section according to Lourens [15] and Lourens et al. [9] identifying marine isotope stages (MIS) 96 to 90. This scheme is continued for the upper section. Correlation is made also with the benthic δ^{18}O record from eastern equatorial Pacific site ODP 849 [26] and with orbital signatures [27].

agreement between reconstructed and actual climate values (for which the correlation coefficients and mean aver age error are 0.95, 1.1 °C for summer temperatures, 0.95, 1.7 °C for winter temperatures, 0.95, 1.1 °C for mean annual temperature, and 0.86, 100 mm for mean annual precipitation, respectively).

Table 1
Pollen taxa identified in the Semaforo record, grouped according to the phytogeographical affinites of the plants [5]

Deciduous forest	Subtropical humid forest	*Centaurea*	Non classified taxa
• *Acer*	• *Cathaya*	Compositae Asteroideae	Abietaceae
• *Alnus*	*Distylium*	Compositae Cichorioideae	Araliaceae
• *Betula*	• *Engelhardia*	Brassicaceae	• *Armeria*
• *Buxus*	*Magnolia*	• Cyperaceae	Boraginaceae
• *Carpinus*	• *Myrica*	• *Ephedra*	Caprifoliaceae
• *Carya*	• *Nyssa*	*Lygeum*	Convolvulaceae
• *Celtis*	Palmae	• Poaceae	*Euphorbia*
• *Cornus*	Sapotaceae	*Phlomis*	Euphorbiaceae
• *Corylus*	*Sciadopitys*	• *Plantago*	Gentianaceae
Elaeagnus	• *Simplocos*	• *Rumex*	*Geranium*
• Ericaceae	• Taxodiaceae	Apiaceae	• *Helianthemum*
• *Eucommia*	*Taxodium*	Meditteranean sclerophyllous forest	• *Knautia*
• *Fagus*	Altitudinal Coniferous forest	*Ceratonia*	Lamiaceae
• *Hedera*	• *Abies*	*Cistus*	Fabaceae
• *Ilex*	• *Cedrus*	*Citrus*	*Lilium*
• *Juglans*	• *Picea*	Cupressaceae	Liliaceae
Liquidambar	*Tsuga*	• *Fraxinus*	Malvaceae
• *Lonicera*	Open vegetation	*Jasminus*	*Nolina*
• *Ostrya*	Amaranthaceae	• *Ligustrum*	Nympheaceae
Parrotia	• Chenopodiaceae	Myrtaceae	Fabaceae Papilionioideae
• *Platanus*	• *Artemisia*	• *Olea*	Plumbaginaceae
• *Populus*	Caryophyllaceae	• *Phillyrea*	• *Potamogeton*
• *Pterocarya*		• *Pinus*	Ranunculaceae
• *Quercus*		• *Pistacia*	Rosaceae
• *Salix*		• *Quercus ilex type*	*Rhus*
• *Sambucus*		• *Rhamnus*	Solanaceae
Taxaceae			• *Sparganium*
• *Tilia*			Tymeleaceae
• *Ulmus*			*Typha*
• *Vitis*			Valerianaceae
• *Zelkova*			

Dots indicate those taxa which are used for palaeoclimate reconstruction.

Specifically, the high correlation coefficients indicate that PCS is able to reliably reproduce trends.

4. Late Pliocene climate

The application of PCS on the Semaforo pollen record allows a detailed view on the Late Pliocene climate development in the Mediterranean, revealing the succession of eight 'interglacials' and nine 'glacials' (Fig. 5). Changes in temperature parameters are mostly correlated with each other ($R^2>0.67$, $p<0.01$), whereas temperature parameters and precipitation are autocorrelated (temperatures leading by ~4 kyr, $R^2>0.47$, $p<0.01$). As compared to temperature parameters, precipitation shows larger relative fluctuations during 'interglacials'. Generally, average oscillations in the transition between 'interglacials' and 'glacials' are higher in mean temperatures of the coldest month (MTC, 7.3 °C) than in mean annual temperatures (MAT, 6.6 °C) and in mean temperatures of the coldest month (MTW, 5.3 °C); mean annual precipitation (MAP) shows an average range of 540 mm. Maximum summer temperatures during the consecutive 'interglacials' vary between 23.8 and 25.1 °C, annual temperatures between 13.2 and 15.5 °C, winter temperatures between 8.0 and 10 °C, and annual precipitation between 985 and 1444 mm. Lowest seasonality and highest oceanicity is revealed for MIS 95 (MTW-MTC is 14.6 °C, MAP is 1444 mm), highest continentality for MIS 81 (MTW-MTC is 16.5 °C). As compared to the present-day climate at Semaforo, during MIS 95, MTW is 2.4 °C, MAT is 1.9 °C, MTC is 3.3 °C, and MAP is 600 mm higher (note that the reconstructions integrates also the climatic signals from high altitude forest elements). Climate conditions during MIS 95 may be most similar to those at present of some regions in Central South China (~24° to 27°N, ~102° to 107°E) and South-Eastern South America (~32° to 36°S, ~54° to 61°E), both regions which are strongly influenced by seasonal reversal (monsoonal) winds. Minimum summer temperatures during the consecutive 'glacials' vary

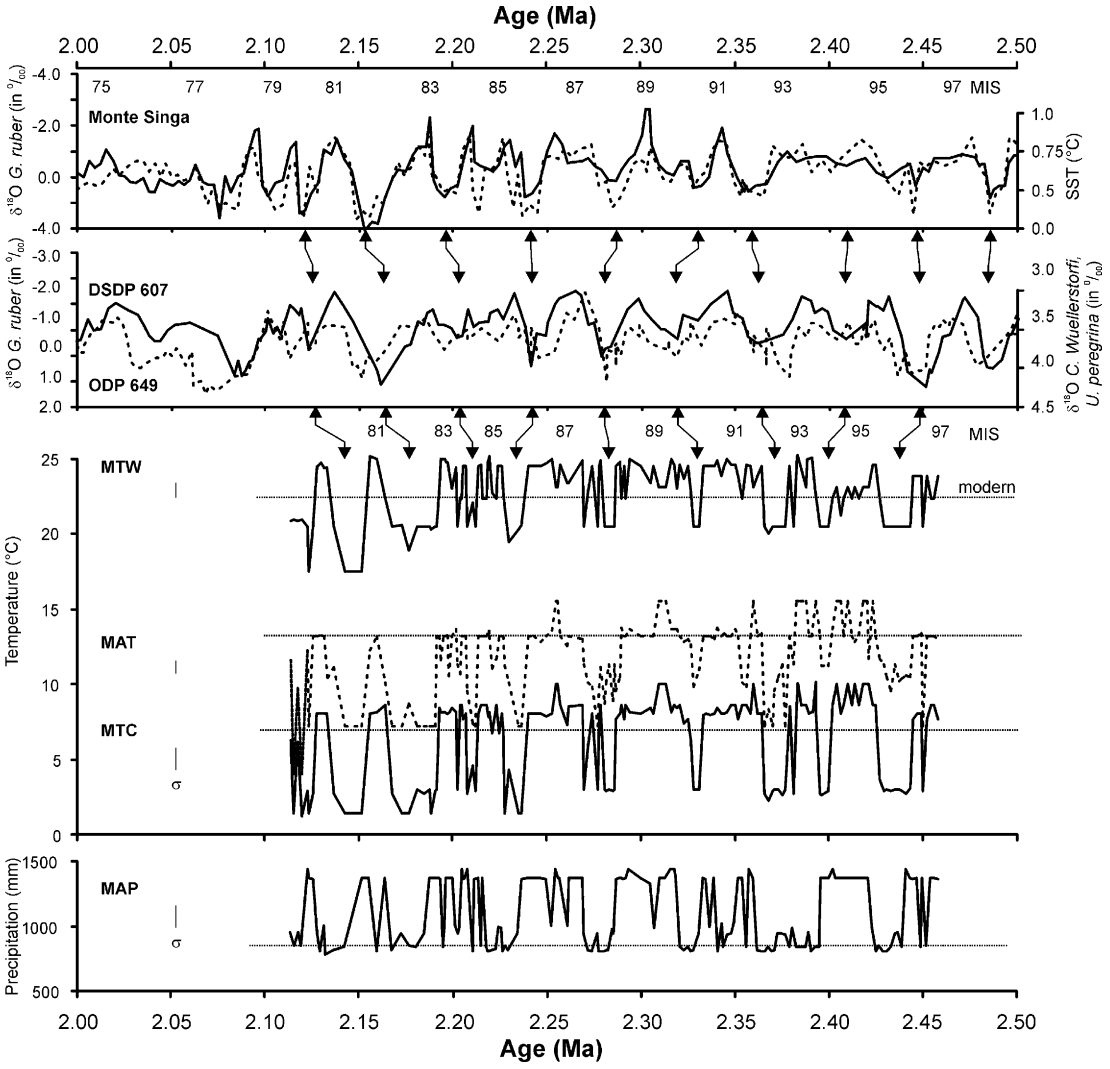

Fig. 5. Climate reconstruction with the PCS method for the Semaforo pollen record, represented by the centres of the mutual climatic ranges for the parameters mean temperature of the warmest month (MTW), mean annual temperature (MAT), mean temperature of the coldest month (MTC) and mean annual precipitation (MAP). Note that although the centres of the probability intervals of PCS point to specific values, it is emphasised that the method basically provides intervals reflecting the ranges of actual palaeoclimate data. Standard deviation (σ) from the centres is 1 °C for MTW, 0.67 °C for MAT, 0.9 °C for MTC, and 166 mm for MAP. Modern climate data at Semaforo (MTW 22.2 °C, MAT 13.6 °C, MTC 6.7 °C and MAP 850 mm) are shown on figure, represented by dotted vertical lines. The climate record is shown together with the planktonic δ^{18}O record, marine isotope stages (MIS), and sea surface temperatures from the Singa section [9], with the benthic δ^{18}O record from DSDP 607 [1] and eastern equatorial Pacific site ODP 849 [26], with obliquity and with precession modulated 65°N June insolation [27].

between 17.5 and 20.5 °C, annual temperatures between 7.2 and 11.2 °C, winter temperatures between 1.4 and 3 °C, and annual precipitation between 780 and 990 mm. Lowest summer, annual, and winter temperatures are found for MIS 80 (MTW-MTC is 16.1 °C). As compared to the present-day climate at Semaforo, during MIS 80, MTW is 4.7 °C, MAT is 6.4 °C, MTC is 5.3 °C, and MAP is 70 mm lower. Climate conditions during MIS 80 may be most similar to those at present of some regions in South France (~44° to 47°N, ~2° to 5°E) and Central West Italy (~42° to 44°N, ~12° to 13°E). The reconstructed values for the 'interglacials' and 'glacials' are reasonably in agreement with estimates for the Mediterranean pollen record of Garraf 1, northeastern Spain [19,29], covering the time window ~5.3 to ~1.75 Ma in 48 pollen samples (10 samples during ~2.5 to ~2 Ma). The deviations between the reconstructed aver-

Table 2
Present-day climate conditions at the localities of Semaforo and Garraf 1 (41°10′N, 2°01′E) with respect to the mean temperature of the warmest (MTW) and coldest month (MTC) in °C, and mean annual precipitation (MAP) in mm

		MTW	MTC	MAP
Present-day	Semaforo	22.2	6.7	850
	Garraf 1	21.4	6.5	690
	gradient S-G	−0.8	−0.2	−160
'Interglacials' maxima	Semaforo	25.0	9.5	1370
	Garraf 1	25.7	9.2	1100
'Glacials' minima	Semaforo	19.8	2.3	830
	Garraf 1	22.0	1.0	600

Average values are calculated for the maxima of the 'interglacials' and minima of the 'glacials' for both records.

age climate values at Garraf 1 and Semaforo largely correspond to the present-day climate gradient between these localities (Table 2). Hence, our reconstructions for that period reflect broad regional climatic patterns.

5. Discussion

The Semaforo pollen record provides an excellent opportunity for the study of the Mediterranean vegetation and climate response on orbital forcing during the Late Pliocene within the time window ~2.46 to ~2.11 Ma. The cyclic vegetation changes recorded in the Semaforo sequence have been proposed to result mainly from variations in temperature and moisture [22,30], affecting shifts in vegetation belts over the Sila Massif 30 km North of Semaforo (palaeoaltitude more than 1500 m [31]) which represents the main pollen source area [32]. In this regard, the change from subtropical forests to open herbaceous formation would reflect the shift from warm and humid 'interglacials' to cold and/or dry 'glacials'. The potential influence of an uplift of the Sila Massif (today 2000 m in altitude) on exposing larger areas for open vegetation (or altitudinal forest) which could influence the palaeoclimate reconstruction, can mostly be disregarded since (1) a constant uplift during the past ~2.46 Ma would result in an uplift of ~70 m during the period covered by the Semaforo record, and (2) there is evidence that the uplift took place after the deposition of marine terraces during or after the middle Pleistocene since these terraces have protected the Semaforo section after its outcrop. Using the PCS method for interpretation of the palaeoclimatic signals reflected by the vegetation, detailed in formation is provided for temperature and precipitation change, suggesting general trends along the successive 'interglacials' and 'glacials'.

5.1. Relationship to orbital parameters and $\delta^{18}O$ data

The spectral analyses on selected vegetation units and on groupings reveal that the vegetation largely responded to the orbital forcing of the ~41 and ~23 kyr periodicities, whereas the ~100 kyr component is weak (Fig. 6a). Interestingly, the obliquity signal is best reflected by subtropical humid forest, altitudinal forest and open herbaceous vegetation, the first of which is also showing a precession component. In contrast, from all the vegetation units, Mediterranean ecosystems and deciduous forest show strongest response to the precession band. With view on groupings of vegetation units (subtropical humid forest+deciduous forest, and subtropical humid forest+altitudinal forest), combined effects are observed in that the spectral patterns of these groups are largely determined by the interference of the spectral patterns of the individual vegetation units. Concerning the reconstructed climatic parameters which interpret the vegetation signals, the spectral analysis suggests a strong control of the ~41 kyr periodicity on variations in temperatures and notably also in precipitation. In contrast, the ~23 kyr periodicity operates stronger on precipitation changes than on temperatures. (Fig. 6b).

5.1.1. Obliquity forcing

The obliquity controlled variations in the Semaforo record, and in the $\delta^{18}O$ data and Sea Surface Temperatures from the Singa section can easily be correlated with the $\delta^{18}O$ records of sites DSDP 607 and ODP 849 (see Fig. 5), therefore arguing to reflect 'interglacial–glacial' cycles bound to ice volume [9]. Based on cross-spectral analysis, the calculated phase relationships reveal that maximum obliquity is closely related to the abundance of warm humid vegetation elements, and to the maxima of pollen derived climate parameters and Singa SST (Fig. 7). For exact phase angles and coherency see Table 3. As a specific pattern, precipitation lags temperature parameters which may be easily seen by comparison of winter temperatures and precipitation for MIS 95, 91, 89, 85 and 83 (Fig. 6). This finding is in agreement with the palynological evidence [16], suggesting warm/dry conditions during the onset of 'interglacials' by the rise of deciduous forest elements, and cold/humid conditions during the onset of 'glacials' by the rise of altitudinal forest elements. If calculating the mean time displacement in the development especially between winter temperatures and precipitation along the 'glacial–interglacial' transitions MIS 96/95 to 82/81 (time of each first sample is taken independently for winter temperatures and precipitation, when

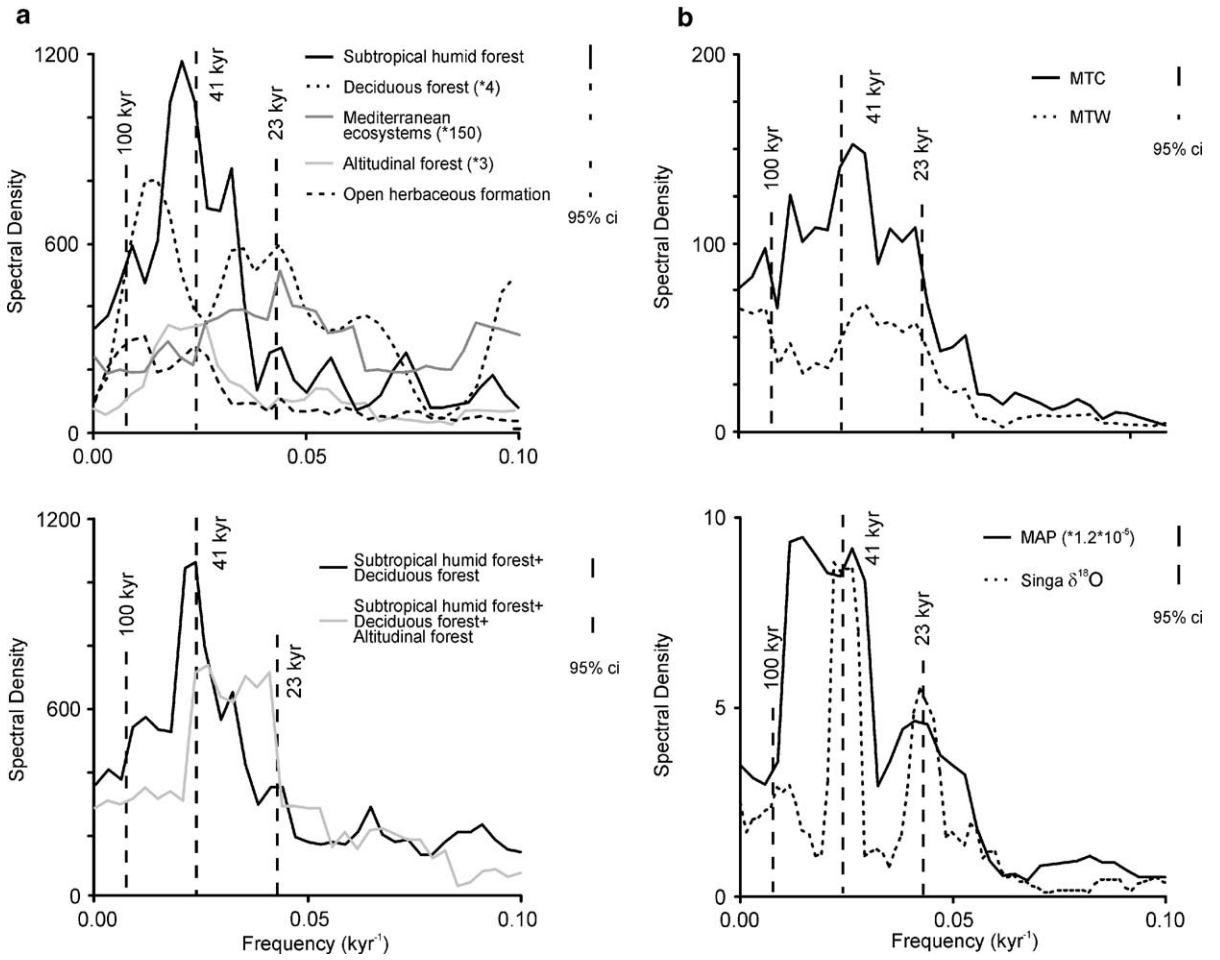

Fig. 6. Power spectra using fast Fourier transformation for different filtered parameters (5% tapered, 7 band Tukey-window). a) Left panel with power spectra for the vegetation units subtropical humid forest, deciduous forest, Mediterranean ecosystems, altitudinal forest and open herbaceous formation, and on the groups. subtropical+deciduous forest and subtropical humid+deciduous+altitudinal forest. b) Right panel with power spectra for the climate parameters mean temperatures of the warmest (MTW) and coldest month (MTC), for mean annual precipitation (MAP), and planktonic $\delta^{18}O$ data from the Singa section for comparison [9]. Confidence intervals (ci) for the parameters shown on figure.

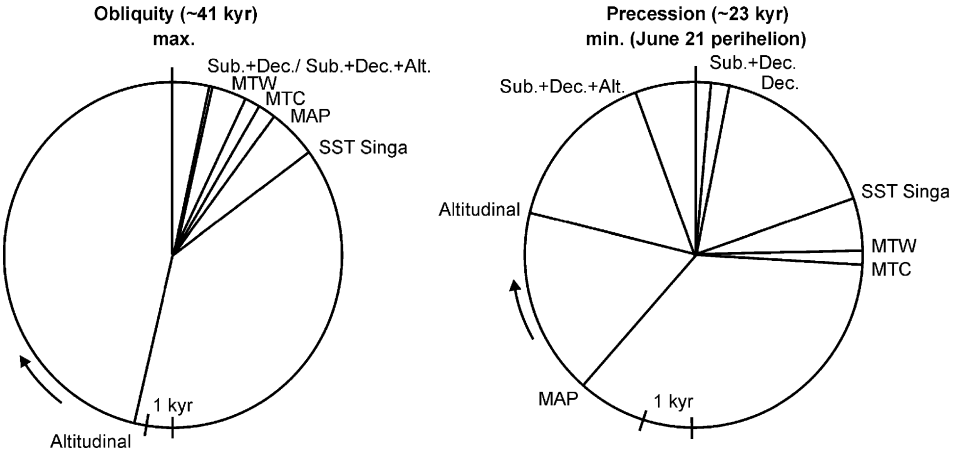

Fig. 7. Cross-spectral analyses using fast Fourier transformation for different filtered parameters (5% tapered, 7 band Tukey-window). Left panel: wheel phase spectrum including different vegetation units, groupings of them, and climate parameter related to obliquity. Right panel: the same for precession.

Table 3
Phase angles in degree (deg.) for the different parameters against obliquity and precession, and coherency (k) (at 95% confidence level)

Parameter	~41 kyr		~23 kyr	
	deg.	k	deg.	k
Subtropical	−12 ± 8	0.87	173 ± 24	0.16
Deciduous	−18 ± 10	0.62	170 ± 3	0.62
Mediterranean	−45 ± 7	0.56	81 ± 3	0.76
Altitudinal	167 ± 3	0.91	−104 ± 2	0.66
Open	156 ± 20	0.47	−173 ± 3	0.37
Sub. + Dec.	−12 ± 4	0.76	175 ± 10	0.49
Sub. + Dec. + Alt.	−12 ± 6	0.73	−162 ± 9	0.61
SST Singa	−52 ± 4	0.41	110 ± 1	0.97
MTC	−30 ± 1	0.69	88 ± 2	0.85
MTW	−25 ± 5	0.66	91 ± 4	0.91
MAP	−37 ± 13	0.59	−41 ± 22	0.96

Parameters include subtropical humid forest (Subtropical, Sub.), deciduous forest (Deciduous, Dec.), Mediterranean ecosystems (Mediterranean), altitudinal forest (Altitudinal, Alt.), open herbacaeous formation (Open), Sea Surface Temperatures of the Singa record (SST Singa), mean temperatures of the coldest (MTC) and warmest month (MTW), and mean annual precipitation (MAP).

8 °C and 1360 mm levels defining the 'interglacials' "plateaus" are exceeded), a value of ~4.0 kyr is obtained (standard deviation ~3.2 kyr, mean time resolution during these transitions is ~1.7 kyr). For the mean time displacement calculated on the consecutive 'interglacial–glacial' transitions MIS 95/94 to 81/80 (when parameter values are below 8 °C and 1360 mm levels), a value of ~3.3 kyr is obtained (standard deviation ~2.0 kyr, mean time resolution during these transitions is ~1.2 kyr). These time lags correspond also to the results provided by a cross-spectral analysis on MTC and MAP, yielding a general phase relationship between these parameters on the obliquity band of ~3.9 ± 0.4 kyr (coherency of 0.9). The time lag between precipitation and temperatures can mainly be explained by means of the SST. During the onset of 'interglacials' sea surface evaporation influencing precipitation is low due to still cool SST, whereas during the onset of 'glacials' still considerable SST allow higher evaporation and precipitation, also supported by lower saturation vapor pressure of the air.

5.1.2. Precession forcing

Since the precession component reflected by the Mediterranean records is almost absent in the $\delta^{18}O$ data of sites DSDP 607 and ODP 849, it can not be interpreted in terms of ice volume changes but was linked to increased Sea Surface Temperatures (SST) at times of sapropel formation related to variations in freshwater input [9,15]. In contrast to the cyclic patterns related to obliquity, the calculated phase relationships on the precession band indicate that precipitation is considerably leading minimum precession (maximum insolation), and is more phase related to altitudinal forest and more in anti-phase with SST, MTW and MTC.

According to the cross-spectral analyses, the maximum phase lag of MAP behind MTC is ~9.6 kyr (coherency of 0.73). As a generalised result, the precession related cycles are determined by the alternation of warm/dry–cold/humid phases. This view deviates from the classical (qualitative) pattern of precession related warm/humid–cold/dry cycles [15]. Our results especially suggest that precession related maximum precipitation mainly corresponds to times of generally low temperatures, which may be explained by (1) increased advection and a presumably more northwestern cyclonic wind regime, and/or (2) enhanced relative humidity due to lower saturation vapor pressure of the colder air.

As a general scheme of the palaeoclimatic development during the period covered by the Semaforo record, it has been considered that the obliquity related warm/humid–cold/dry cycles are superimposed by the precession related warm/dry–cold/humid cycles.

5.2. Long-term climatic trends

The reconstructed climate data are analysed for general trends calculating linear regressions for climate parameters along the eight 'interglacials' and nine 'glacials', that is for the development of 'interglacial' maxima, 'glacial' minima, and 'interglacial–glacial' amplitudes. Unlike the various marine palaeoclimate indices which reveal no obvious characteristics along MIS 97 to MIS 80, the vegetation based climatic analysis suggests different long-term trends of atmospheric change in the Mediterranean.

5.2.1. Annual and winter cooling along consecutive 'interglacials'

The coldest 'interglacial' MIS 81 is even warmer in summer temperatures of ~3 °C, in winter temperatures of ~2 °C, and with higher precipitation of ~500 mm than the modern climate conditions at Semaforo. Referring to the analysis of the 'interglacials' maxima along MIS 95 to 81 (total period of ~280 kyr), strong trends of decreasing annual temperatures of ~2.8 °C and winter temperatures of ~2.3 °C become obvious (Fig. 8a). Due to similar summer temperatures, seasonality is increasing during the consecutive 'interglacials' by ~2.3 °C. Although the general decrease of subtropical humid elements and their replacement by decidu-

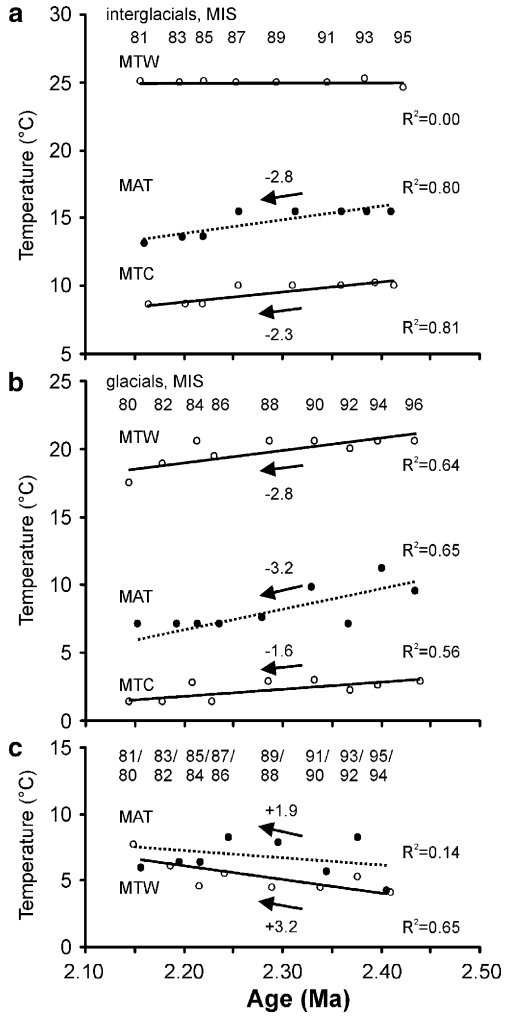

Fig. 8. Linear climatic trends along the consecutive 'interglacials' MIS 97 to 81 and 'glacials' MIS 96 to 80 in the Semaforo record for the parameters mean temperature of the warmest month (MTW), mean annual temperature (MAT) and mean temperature of the coldest month (MTC), related to timescale. (a) Maximum values during the 'interglacials'. (b) Minimum values during the 'glacials'. Coefficients of determination (at significance level $p<0.01$) for regressions, and resulting total changes between the lower and upper part of the record are shown on figure. (c) Maximum 'interglacial–glacial' amplitudes (difference between 'interglacial' maximum and succeeding 'glacial' minimum values).

ous forest elements [22], the annual precipitation shows no trend. This can be explained by the following: (1) the occurrence of subtropical humid elements during all 'interglacials' (abundance > 6%) indicate warm and (year-long) humid climate conditions at all [5,19,33–36]. (2) The subtropical humid elements are more sensitive to temperature changes rather than precipitation changes, as can be interpreted from the Semaforo and Vrica composite section (Crotone, Italy) spanning the period from ~2.4 to ~1.2 Ma. There, Taxodiaceae are gradually replaced by *Cathaya* between ~2.4 and ~2.0 Ma, and *Cathaya* is replaced by *Tsuga* after ~1.4 Ma [5,30]. Today, however, these taxa can be found at different altitudes with *Cathaya* and *Tsuga* at higher levels than Taxodiaceae, but all requiring similar levels of high humidity . The finding of decreasing winter temperatures is further in agreement with estimates derived from the northern German record of Lieth (53°43′N, 9°38′E) covering MIS 97 to 81 in about 49 pollen samples, based on the same reconstruction method [37]. It has been proposed for Lieth a gradual decrease in winter temperatures of ~5 °C during the consecutive 'interglacials', and also an increase in summer temperatures of ~1 °C. Regardless of the difference in the reconstructed absolute decreases in winter temperatures at Semaforo and Lieth, the comparison emphasises the over-regional character of the determined trend along the consecutive 'interglacials' during the period considered.

5.2.2. General cooling along consecutive 'glacials'

Strong cooling trends are also observed along 'glacials' MIS 96 to 80 (period of ~300 kyr) for all temperature parameters, with decreasing summer temperatures of 2.8 °C, mean annual temperatures of 3.2 °C, and winter temperatures of 1.6 °C (Fig. 8b). This finding coincides with the general increase of altitudinal forest elements and open vegetation elements, but does not reveal enhanced aridity. Considering the different marine indices, only the $\delta^{18}O$ data from the Singa record exhibits a weak trend of increasing values along MIS 96 to MIS 78 (+1.3‰, $R^2=0.4$). Our results are also in agreement with the pollen based reconstructions from the record of Lieth, where a decrease in winter temperatures of ~5.5 °C along MIS 96 to 80 is suggested [37]. The intensified cooling during the consecutive obliquity dominated 'glacials' may correspond to the strong imprint of the obliquity signal caused by the control meridional temperature gradients exert on the poleward transport of moisture, allowing to progressively build-up Northern Hemisphere ice sheets [38]. It may also be related to intensified atmospheric circulation [39], or to enhanced ice-rafting as evidenced from records in the Norwegian Sea and North Atlantic during 'glacials' and 'interglacial–glacial' transitions [40].

5.2.3. Increasing amplitudes of consecutive 'interglacial–glacial' transitions

Calculating the maximum climatic amplitudes between consecutive 'interglacials' (maximum values are considered) and 'glacials' (minimum values are considered), another trend suggests increasing summer tem-

perature amplitudes of ~3.2 °C and mean annual temperatures of ~1.9 °C along MIS 96/95 to 81/80 (Fig. 8c). For comparison, the analysis on the $\delta^{18}O$ data from the Singa record reveals a trend suggesting higher amplitudes along MIS 97/96 to MIS 79/78 (+2.4‰, $R^2=0.6$), which is not obvious from the $\delta^{18}O$ record at DSDP 607 in the North Atlantic. It is especially suggested that changes in global ice volume associated with reductions in the Mediterranean surface-water salinity (resulting from changes in the rates of evaporation/precipitation and from fluvial runoff), led to higher 'interglacial–glacial' amplitudes in the region [41,42]. As compared to the amplitude of winter temperature change of more than 18 °C during the last 'interglacial–glacial' transition (Eemian–Weichselian) as reconstructed from the pollen record of Lago Grande di Monticchio/Southern Italy [43], the Late Pliocene transitions show less than half in amplitude.

6. Conclusions

The quantitative climate analysis of the Mediterranean pollen record of Semaforo/Southern Italy provides new and detailed information on the climate development along eight Late Pliocene 'interglacials' and nine 'glacials' during the time window 2.46–2.11 Ma. Mainly forced by the obliquity and the precession signal modulating 65°N June insolation, the analysis of climate development reveals specific characteristics of change.

(1) Summer, mean annual and winter temperatures, as well as precipitation are considerably higher during the Late Pliocene subtropical humid 'interglacials' as compared to present-day climate conditions in the study area. Temperatures during 'glacial' periods are lower, but precipitation is similar than at present.
(2) Relying on the timescale of the Semaforo record, the spectral analyses on vegetation units and on reconstructed climate parameters reveals the considerable imprint of the ~41 kyr obliquity and ~23 kyr precession periodicity. Generalised, it is evidenced the alternation of warm/humid–cold/dry 'interglacial–glacial' cycles on the obliquity band, which are superimposed by warm/dry–cold/humid cycles on the precession band. Whereas the obliquity bound climatic cycles in the Mediterranean largely follows the global change in ice volume, the precession related cycles may be best explained by the influence of warm/dry southern anticyclonic wind circulation alternating with a cold/humid northwestern cyclonic wind regime.
(3) A time lag of ~4 kyr is observed in the development of temperatures and precipitation during the obliquity controlled 'glacial–interglacial' cycles, and of ~9.6 kyr in maximum during the precession related cycles, with precipitation lagging temperature parameters. Transitional phases are thus characterised by warm/dry or cold/humid conditions.
(4) Along the consecutive 'interglacials' no precipitation trend change is yielded according to the abundance of taxa requiring a high amount of year-long humidity.
(5) A strong trend in the climate development of over-regional scale along the consecutive Late Pliocene 'interglacials' is indicated by the reduction in minimum mean annual and winter temperatures, and by the intensification of seasonality.
(6) A further trend in the climate development along the consecutive 'glacials' is indicated by reduced minimum summer, mean annual, and winter temperatures.
(7) Considering maximum temperature shifts along the consecutive 'interglacial–glacial' transitions, the amplitudes are increasing for summer and mean annual temperatures. As compared to the amplitude of winter temperature change during the last 'interglacial–glacial' (Eemian–Weichselian) transition in South Italy, the Late Pliocene shifts are less than half in size.

Acknowledgements

S. Klotz and D. Uhl gratefully acknowledge the financial support by the Alexander von Humboldt-Foundation, and N. Combourieu-Nebout by CNRS for processing palynological samples (this is LSCE contribution No. 1804). S. Klotz gratefully acknowledges also the financial support by the Laboratoire PaléoEnvironnements and PaléobioSphère, and the European Science Foundation. The authors thank Dr. L. Lourens, Prof. C. Tzedakis and an anonymous reviewer for their valuable comments on an earlier manuscript which helped to improve the manuscript.

References

[1] M.E. Raymo, W.F. Ruddiman, J. Backman, B.M. Clement, D.G. Martinson, Late Pliocene variation in Northern Hemisphere ice sheets and North Atlantic deep circulation, Palaeoceanography 4 (1989) 413–446.
[2] N.J. Shackleton, New data on the evolution of Pliocene climatic variability, in: E.S. Vrba, G.H. Denton, T.C. Partridge (Eds.), Paleoclimate and Evolution, with Emphasis on Human Origins, Yale Univ. Press, New Haven, 1995, pp. 24–45.

[3] J. Zachos, M. Pagani, L. Sloan, E. Thomas, K. Billups, Trends, rhythms, and aberrations in global climate 65 Ma to present, Science 292 (2001) 686–693.
[4] W.H. Zagwijn, Subtropical relicts in the Pliocene flora of Brunssum (The Netherlands), Geol. Mijnb. 69 (1990) 219–225.
[5] N. Combourieu-Nebout, C. Vergnaud Grazzini, Late Pliocene northern hemisphere glaciation: the continental and marine responses in the central Mediterranean, Quat. Sci. Rev. 10 (1991) 319–334.
[6] J.P. Suc, Origin and evolution of the Mediterranean vegetation and climate in Europe, Nature 307 (1984) 429–432.
[7] C. Vergnaud Grazzini, J.F. Sallège, M.J. Urrutiaguer, A. Iannace, Oxygen and Carbon isotope stratigraphy of ODP hole 653A and site 654: the Pliocene–Pleistocene glacial history recorded in the Tyrrhenian Basin (West Mediterranean), Proc. Ocean Drill. Prog., Sci. Results 107 (1990) 361–385.
[8] R.C. Thunell, D.F. Williams, E. Tappa, D. Rio, I. Raffi, Pliocene–Pleistocene stable isotope record for ocean drilling program site 653, Tyrrhenian Basin, implications for the paleoenvironmental history of the Mediterranean Sea, Proc. Ocean Drill. Prog., Sci. Results 107 (1990) 387–399.
[9] L.J. Lourens, F.J. Hilgen, L. Gudjonsson, W.J. Zachariasse, Late Pliocene to early Pleistocene astronomically forced sea surface productivity and temperature variations in the Mediterranean, Mar. Micropaleontol. 19 (1992) 49–78.
[10] L.J. Lourens, A. Antonarakou, F.J. Hilgen, A.A.M. Van Hoof, C. Vergnaud-Grazzini, W.J. Zachariasse, Evaluation of the Plio-Pleistocene astronomical timescale, Paleoceanography 11 (1996) 391–413.
[11] D. Kroon, I. Alexander, M. Little, L.J. Lourens, A. Matthewson, A.H.F. Robertson, T. Sakamoto, Oxygen isotope and sapropel stratigraphy in the Eastern Mediterranean during the last 3.2 million years, Proc. Ocean Drill. Prog., Sci. Results 160 (1998) 181–189.
[12] W.H. Zagwijn, Aspects of the Pliocene and early Pleistocene vegetation in the Netherlands, Meded. - Rijks Geol. Dienst C 3 (1960) 1–78.
[13] J.-P. Suc, A. Bertini, N. Combourieu Nebout, F. Diniz, S. Leroy, E. Russo-Ermolli, Z. Zheng, E. Bessais, J. Ferrier, Structure of West Mediterranean vegetation and climate since 5.3 Ma, Acta Zool. Cracov. 38 (1995) 3–16.
[14] F.J. Hilgen, Astronomical calibration of Gauss to Matuyama sapropels in the Mediterranean and implications for the geomagnetic polarity time scale, Earth Planet. Sci. Lett. 104 (1991) 226–244.
[15] L.J. Lourens, Astronomical Forcing of Mediterranean Climate during the Last 5.3 Million Years, Proefschrift, Universiteit Utrecht, Utrecht, 1993, 247 pp.
[16] N. Combourieu-Nebout, Vegetation response to upper Pliocene glacial/interglacial cyclicity in the central Mediterranean, Quat. Res. 40 (1993) 228–236.
[17] J. Iversen, Viscum, Hedera and Ilex as climate indicators, Geol. Fören. Stöckh. Forh. 66 (1944) 463–483.
[18] K.J. Sinka, T.C. Atkinson, A mutual climatic range method for reconstructing palaeoclimate from plant remains, J. Geol. Soc. 156 (1999) 381–396.
[19] S. Fauquette, J. Guiot, J.P. Suc, A method for climatic reconstruction of the Mediterranean Pliocene using pollen data, Palaeogeogr. Palaeoclimatol. Palaeoecol. 144 (1998) 183–201.
[20] S. Klotz, Neue Methoden der Klimarekonstruktion-angewendet auf quartäre Pollensequenzen der französischen Alpen, Tüb. Mikropaläontol. Mitt. 21 (1999) (169 pp.).
[21] S. Klotz, U. Müller, V. Mosbrugger, J.L. de Beaulieu, M. Reille, Eemian to early Würmian climate dynamics: history and pattern of changes in Central Europe, Palaeogeogr. Palaeoclimatol. Palaeoecol. 211 (2004) 107–126.
[22] N. Combourieu-Nebout, Réponse de la végétation de l'Italie méridionale au seuil climatique de la f in du Pliocène d'apres l'analyse pollinique haute résolution de la section Semaforo (2,46 à 2,1 Ma), C.R. Acad. Sci. Paris 321 (1995) 659–665.
[23] L.J. Lourens, F.J. Hilgen, N.J. Shackleton, J. Laskar, D. Wilson, The Neogene period, in: F.M. Gradstein, J.G. Ogg, A.G. Smith (Eds.), A Geologic Time Scale 2004, Cambridge University Press, 2004, pp. 409–440.
[24] G. Pasini, M.L. Colalongo, The Pleistocene boundary stratotype at Vrica, Italy, in: J.A. Van Couvering (Ed.), The Pleistocene Boundary and the Beginning of the Quaternary, Cambridge University Press, Cambridge, 1997, pp. 15–45.
[25] K. Faegri, J. Iversen, Textbook of Pollen Analysis, Hafner Press, New York, 1997, 295 pp..
[26] A.C. Mix, N.G. Pisias, W. Rugh, J. Wilson, A. Morey, T.K. Hagelberg, Benthic foraminifer stable isotope record from Site 849 (0–5 Ma): local and global climate changes, Proc. Ocean Drill. Program Sci. Results 138 (1995) 371–412.
[27] J. Laskar, P. Robutel, F. Joutel, M. Gastineau, A. Correia, B. Levrand, A long-term numerical solution for the insolation quantities of the Earth, Astron. Astrophys. 428 (2004) 261–285.
[28] S. Klotz, J. Guiot, V. Mosbrugger, Continental European Eemian and early Würmian climate evolution: comparing signals using different quantitative reconstruction approaches based on pollen, Glob. Planet. Change 36 (2003) 277–294.
[29] J.-P. Suc, J. Cravatte, Etude palynologique du Pliocène de Catalogne (nord-est de l'Espagne), Paléobiol. Cont. 13 (1982) 1–31.
[30] N. Combourieu-Nebout, S. Fauquette, P. Quézel, What was the late Pliocene Mediterranean climate like: a preliminary quantification from vegetation, Bull. Soc. Géol. France 171 (2000) 271–277.
[31] W. Landini, E. Menesini, L'ittiofauna plio-pleistocenica della sezione delle Vrica (Crotone-Calabria), Bull. Soc. Palaeontol. Ital. 17 (1978) 143–175.
[32] V.F. Rögl, F.F. Steininger, Vom Zerfall der Tethys zu Mediterran und Paratethys. Die Neogene Paläogeographie und Palinspastik des zirkummediterranean Raumes, Ann. Naturhist. Mus. Wien 85 (1983) 135–163.
[33] C.W. Wang, The Forests of China with a Survey of Grassland and Desert Vegetation, Maria Moors Cabot Foundation, Cambridge, Mass., 1961.
[34] L.E. Heusser, W.L. Balsam, Pollen distribution in the northwest Pacific Ocean, Quat. Res. 7 (1977) 45–62.
[35] J.L. Vankat, The Natural Vegetation of North America: An Introduction, Wiley, New York, 1979.
[36] S. Fauquette, J.-P. Suc, J. Guiot, F. Diniz, N. Feddi, Z. Zheng, E. Bessais, A. Drivaliari, Climate and biomes in the West Mediterranean area during the Pliocene, Palaeogeogr. Palaeoclimatol. Palaeoecol. 152 (1999) 15–36.
[37] J. Pross, S. Klotz, Palaeotemperature calculations from the Praetiglian/Tiglian (Plio-Pleistocene) pollen record of Lieth, northern Germany: implications for the climatic evolution of NW Europe, Glob. Planet. Change 34 (2002) 253–267.
[38] M.E. Raymo, K.H. Nisancioglu, The 41 kyr world: Milankovitch's other unsolved mystery, Paleoceanography 18 (2003), doi:10.1029/2002PA000791.

[39] S. Leroy, L. Dupont, Development of vegetation and continental aridity in northwestern Africa during the Late Pliocene: the pollen record of ODP Site 658, Palaeogeogr. Palaeoclimatol. Palaeoecol. 109 (1994) 295–316.
[40] K. McIntyre, M.L. Delaney, A.C. Ravelo, Millenial-scale climate change and oceanic process in the late Pliocene and early Pleistocene, Paleoceanography 16 (2001) 535–543.
[41] M.W. Howell, R.C. Thunell, E. Di Stefano, R. Sprovieri, E.J. Tappa, T. Sakamoto, Stable isotope chronology and paleoceanographic history of Sites 963 and 964, Eastern Mediterranean Sea, Proc. Ocean Drill. Prog., Sci. Results 160 (1998) 167–180.
[42] F.J. Hilgen, L.J. Lourens, A. Berger, M.F. Loutre, Evaluation of the astronomically calibrated time scale for the late Pliocene and earliest Pleistocene, Paleoceanography 8 (1993) 549–565.
[43] J.R.M. Allen, W.A. Watts, B. Huntley, Weichselian palynostratigraphy, palaeovegetation and palaeoenvironment, the record from Lago Grande di Monticchio, Southern Italy, Quat. Int. 73/74 (2000) 91–110.